Modeling and Characteristics of Nanostructured NiO/GeSe core-shell Perovskite Solar Cell

AWAD KHALED[1], MOHAMED FARHAT O. HAMEED[1,2,3*], MOHAMED HUSSIEN[1,4,5], K. T. V. GRATTAN[6], B. M. A. RAHMAN[6], AND S. S. A. OBAYYA[1*]

[1] Centre for Photonics and Smart Materials, Zewail City of Science and Technology, October Gardens, 6th of October City, Giza 12578, Egypt.
[2]Nanotechnology and Nanoelectronics Engineering Program, Zewail City of Science and Technology, October Gardens, 6th of October City, Giza 12578, Egypt.
[3]Mathematics and Engineering Physics Department, Faculty of Engineering, University of Mansoura, Mansoura 35516, Egypt.
[4]Department of Physics, Faculty of Science, Ain Shams University, Abbassia 11566, Cairo, Egypt
[5]Light Technology Institute, Karlsruhe Institute of Technology, Engesserstrasse 13, 76131 Karlsruhe, Germany
[6]Department of Electrical and Electronic Engineering, City, University of London, London EC 1 V 0HB, United Kingdom
**Corresponding author: sobayya@zewailcity.edu.eg, mfarahat@zewailcity.edu.eg*

Inorganic-organic hybrid Perovskite Solar Cells (PSCs) have recently seen considerable progress and this has encouraged researchers to evolve and test numerous different and potentially improved device architectures. As a result, in this paper, a theoretical design for improving light absorption to obtain maximum photocurrent using NiO/GeSe core-shell nanostructures has been introduced. The effects of using nanostructures arrays, based on the light trapping technique, on the light absorption, generation of carriers, absorption field profiles, and finally the photocurrent density of PSCs have been investigated, through a three-dimensional (3D) finite difference time domain (FDTD) approach. By selecting NiO and GeSe as the core and the shell materials, the absorption of the active layer has been increased, relative to the use of a conventional planar structure. This core-shell nanostructure leads to a reduction in the carrier recombination within the PSC proposed design. The results obtained from a simulation carried out have shown that the device performance is highly dependent on the height and materials used in the core-shell. Significantly, an optimal height of 160 nm was obtained for core-shell in a PSC design with a J_{ph} value of 27.23 mA/cm^2.

1. INTRODUCTION

Currently there is an unprecedented increase in the use of renewable energy resources. The transition from fossil fuel resources to clean and sustainable resources is widely recognized as a vital part in what must be a revolution in the way energy is generated and used. Solar energy is considered as the superior clean energy source, as it is abundant, non-polluting and widely available. Photovoltaic technology (PV) is seen as the most promising, with the aim being to decrease the amount of the silicon (Si) used in PVs, to reduce the overall cost. Thin film solar cells (TFSCs) with a thickness of a few micrometers can allow this to be achieved [1-4]. Recently, different diffractive and plasmon structures have been introduced to boost the absorption and energy conversion efficiencies of such SCs, using for example nanowires [5], nanopillars [6], nanoholes [7], nanopyramids [8], nanocones [9], or nanostars [10], for example. Moreover, other studies have used nanostructures, formed from dielectrics inside the active layer [11-13], or metal nanoparticles to improve the absorption characteristics in many types of SCs [14, 15]. However, the incorporation of organic materials and C-Si creates a conductive effect, and this has several advantages, such as a simple manufacturing processes, superior mechanical properties, low temperature processing and, overall, a low cost [16, 17]. In a recent publication, Duan et *al.* have reported a high performance organic-nanostructured Si SC with an efficiency of 14.08% [18].

Perovskite has been studied intensively in photovoltaic applications since the first use of a Perovskite Solar Cell, taking advantage of a promising device efficiency and affordable cost [19, 20]. The active layer of perovskite has two important features: high energy conversion efficiency and low cost of the manufacturing process. Various other features of perovskite materials have made them attractive for photovoltaics, such as a high absorption of the light spectrum, tunability of the bandgap, the easy facility for material synthesis and device fabrication, a low carrier recombination rate and a large diffusion length of the carriers [21-25]. Perovskite Solar Cells (PSCs) absorb light over a wavelength range from 300 to 800 nm. The latest value for the ECE for Perovskite Solar Cells (PSCs) to be reported is 25.5 % (a measurement certified by the National Renewable Energy Laboratory (NREL) as reported by KRICT/MIT [26]). However, PSCs have absorption limitations at longer wavelengths due to the low thickness of the active layer. Also, although the absorption coefficient of PSCs is high, it falls by 90% at wavelengths >650 nm [27]. In this regard, the semiconductors of Group IV-VI, which have a narrow energy band, provide a significant opportunity for PV applications [28]. In particular, GeSe can be a very suitable candidate for the use as SC components, taking advantage of its high chemical stability. This material has an experimental energy band of 1.1 eV, which makes it well suited for active absorption of light in different applications of SCs [29].

There are three main parts in a typical PSC, namely the Perovskite active layer, the hole transport layer (HTL), and the electron transport layer (ETL). In recent work, researchers have reported using spiro-OMeTAD and TiO_2 as the materials for the HTL and ETL, respectively. However, the spiro-OMeTAD causes corrosion of the Perovskite because of its unstable nature, and its decomposition caused by UV radiation, limits the widespread usage of PSCs using this material [30]. Therefore, it is vital to select the most suitable HTL material and create an optimal structure to improve the performance of the PSCs, to tackle most effectively the existing challenges. Scientists and researchers have also been focusing on other HTL materials for use in high efficiency SCs and here inorganic HTL materials, such as NiOx, NiO and CuSCN have gained considerable attention, due to their low costs and high chemical stability [31, 32]. Inorganic hole transport layers, based on copper, have various merits such as high chemical stability, high conductivity and

high hole mobility [33], as seen in the work of Grätzel who used copper thiocyanate (CuSCN) as an effective and cheap p-type inorganic material, to reach a PCE of ~12.4% [34]. Further, Arora et *al.* have suggested a layer of reduced graphene between the back contact and the HTL to improve the PSCs stability, with +1000 h of operational time stability [35]. In particular, recent techniques for improving the efficiency of PSCs have been based on using silica nanospheres in an antireflective coating [36, 37], designing the front nanoarchitectures by use of nanophotonics [38], or nanostructures based on plasmonic materials above the metal back contact [39].

Currently, dielectric nanostructures have been seen as favorable alternatives to plasmonic nanostructures [40-42]. Many of the dielectrics used in the optical wavelength range are semi- or fully transparent, producing negligible losses within the dielectric nanostructures. Furthermore, the dielectrics used, with their high refractive index, enable good control over the direction of the light at the nanoscale, achieved by tuning the Mie resonance of the nanostructures. Such tuning of the Mie resonance of the absorption could then change the minimum wavelength of the reflected light. Also, the process of changing the Mie resonance scattering enables the light coupling into the substrate waveguide modes. In this regard, titanium dioxide (TiO_2) is considered to be one of the best, most commonly used materials for various types of SCs, because of its high refractive index ($n \approx 2.7$), low optical losses in the wavelength range of the visible to near-infrared [12], and prospect of tuning its Mie resonance by varying the shape and dimensions of the nanostructures. For example, Jin et *al.* used the deposition method of the low temperature solution to synthesize CuSCN as the HTL [43] and after choosing the most suitable HTL material, an optimum structure will be proposed for this layer in this work. To improve the device efficiency, it is necessary to increase the active layer absorption, to allow nanostructures to be used in the active layer for light trapping (LT).

The light absorption mechanism in these SCs could be improved by integrating the light trapping structures, where the light is absorbed (exponentially from front to back in the bulk semiconductor). The use of core-shell nanostructures leads to an improvement of the PSC efficiency, where such an improvement is due to the enhancement of interface contact between the core-shell nanostructures and the Perovskite layer, and charge recombination suppression [44]. Inserting core-shell nanostructures would facilitate the efficient use of different materials which have a short diffusion length. Furthermore, they would minimize the device production cost and time, due to the use of thin absorbing layers [45]. The presence of carrier recombination at the surface of GeSe-CuSCN arises because of the valence band (Ev) mismatch and the low hole injection efficiency into the GeSe, which using the nanostructures of the core-shell, can aid finding a solution to this problem and consequently an increase in the efficiency of the PSC. According to the results acquired, unstable charge transfer may be caused by the low hole mobility at the GeSe layer in the PSC. In the case of a p-type direct bandgap semiconductor (Eg=3.8 eV), other PSCs have been introduced with NiO. Also, this material has a valence band Ev=5.1 eV and thus can facilitate hole transfer from the GeSe layer to the main HTL (CuSCN layer), due to an improvement of the charge transfer process inside the GeSe, as well as a reduction of the recombination rate in this area.

In this study, a modified approach to the core-shell structure is proposed, to improve the PSC efficiency, and simulate a PSC on NiO/GeSe core-shell design, based on nanowires (NWs), nanocones, inverted nanocones, truncated cones, inverted truncated cones, two designs of a funnel shape and inverted funnel shapes. Specifically, the optical absorption and the generation levels of the electron-hole were investigated, following which planar PSCs were compared with the nanostructures of the core-shell. In addition, different shapes, dimensions and heights have been studied, with a view to optimizing the effect of elevation changes on the absorption A(λ), generation of the carriers, the collection of carriers and the photocurrent density (J_{ph}). The different nanostructures suggested offer high values of J_{ph} of 23.86 mA/cm^2, 25.34 mA/cm^2, 27.23 mA/cm^2, 26.18 mA/cm^2, 27.02 mA/cm^2, 24.10 mA/cm^2, 25.57 mA/cm^2, 24.57 mA/cm^2, and 26.33 mA/cm^2, results which are favorable compared to 18.70 mA/cm^2 for the conventional PSC.

2. Design consideration and Simulation Strategy

Figure 1 shows the planar PSC studied, a PSC with different core shell nanostructures, such as cylindrical, nanocone, truncated cone, and funnel NWs types. The conventional PSC consists of (from top to the bottom) the following: a transparent conductive oxide (ITO), a ETL layer as incorporating of titanium dioxide (TiO_2), a Perovskite ($CH_3NH_3PbI_3$) active layer, a HTL layer from CuSCN, NiO as the core, and GeSe as the shell, in the core-shell design, and finally an Au-based back reflector. The PSC discussed has a width of 200 nm and also the thickness of the ITO, TiO_2, $CH_3NH_3PbI_3$, CuSCN, and Au layers are taken to be 50 nm, 50 nm, 200 nm, 600 nm, and 100 nm, respectively. The initial geometrical parameters of the core-shell nanostructures are listed in Tables 1 and 2. The heights of the core-shell nanostructures are also optimized at a constant volume. The three-dimensional (3D) simulations carried out were performed using the Finite Difference Time Domain (FDTD) approach, through the use of via Lumerical software package [46]. A plane wave source has been used above the ITO as the source of the illuminating 'sunlight'. The incident light source has a AM 1.5 solar spectral irradiance, through the wavelength range from 300 to 1000 nm. To reduce the computational time, a single unit cell has been modeled, with the inclusion of periodic boundary conditions. Also, a perfectly matched layer (PML) has been employed along the z-direction in the top and bottom boundaries, to remove unnecessary reflections. The absorption A(λ) is here defined as the portion of the absorbed incident light in the PSC at wavelength, λ, which could be evaluated from the value of the transmission, T(λ), and the reflection, R(λ), as follows

$$A(\lambda) = R(\lambda) - T(\lambda) \qquad (1)$$

The values of T(λ) and R(λ) were calculated by using two monitors, one below and another above the active material, as shown in Fig. 1(f). The complex refractive indices of the materials used were taken from the previously published studies such as ITO [47], CuSCN [48], $CH_3NH_3PBI_3$ [49], TiO_2 [50], NiO [51], and GeSe [52]. In this study the photocurrent density (J_{ph}) was used as a suitable function to quantify the broadband absorption ability of the proposed PSC where:

$$J_{ph} = \frac{e}{hc} \int_{300nm}^{1000nm} \lambda \, Fs(\lambda) \, Pabs(\lambda) \, d\lambda \qquad (2)$$

and here e is the charge of the electron, h is Plank's constant, Fs (λ) is the photon flux density in the AM 1.5 solar spectral irradiance and Pabs is the optical absorption. Next, through the use of the FDTD model, the electric field was calculated; then the optical electron-hole pairs generation rate could be obtained inside the active layer (as [57]) from:

$$G_{opt} = \frac{\varepsilon'' E^2}{2\hbar} \qquad (3)$$

where G_{opt} is proportional to the electric field intensity (E) and the imaginary part of the permittivity (ε''). Based on Eq. (3), the generation rate (G) and the electric field (E) were increased by increasing the incident light absorption.

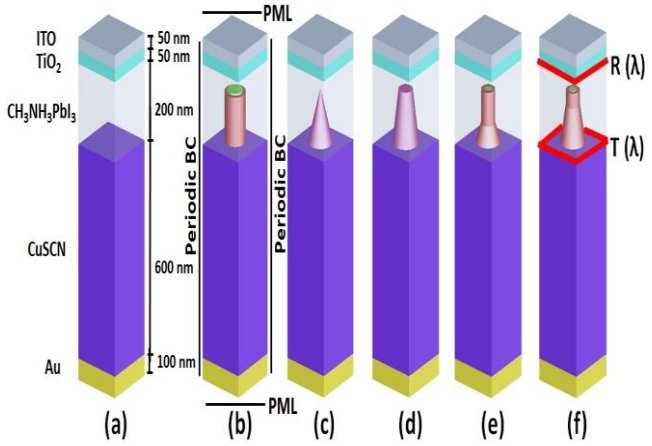

Fig.1. (a) Planar PSC, and PSC with (b) cylindrical nanowire, (c) nanocone NW, (d) truncated NW, (e) first funnel NW, and (f) second funnel NW.

Table 1. The geometrical parameters of the nanostructures at the same volume

Structure	Core		Shell	
	Top radius (nm)	Bottom radius (nm)	Top radius (nm)	Bottom radius (nm)
Cylindrical nanowire	25	25	50	50
Cone	0	43	0	86
Inverted cone	43	0	86	0
Truncated cone	20	30	35	65
Inverted truncated cone	30	20	65	35

Table 2. The geometrical parameters of the funnel core-shell

Structure	Cylindrical core (nm)		Cylindrical shell (nm)		Cone core (nm)		Cone shell (nm)	
	Top radius	Bottom radius	Top radius	Bottom radius	Top radius	Bottom radius	Top radius	Bottom radius
Funnel	20	20	35	35	20	30	35	65
Inverted funnel	20	20	35	35	30	20	65	35

3. Numerical Results and Discussion

The nanostructures considered can be used to increase the light trapping through the active layer and hence the generation rate, as shown in Fig. 1. In this context, the nanostructures periodicity should be shorter than the smallest wavelength, to enhance the absorption, the generation of the electron-hole pairs, and hence the value of J_{ph}. The carrier transfer can be also improved by increasing the electric field. In addition, the collection of carriers can be improved by increasing hole transport layer (HTL) contact region with the active layer.

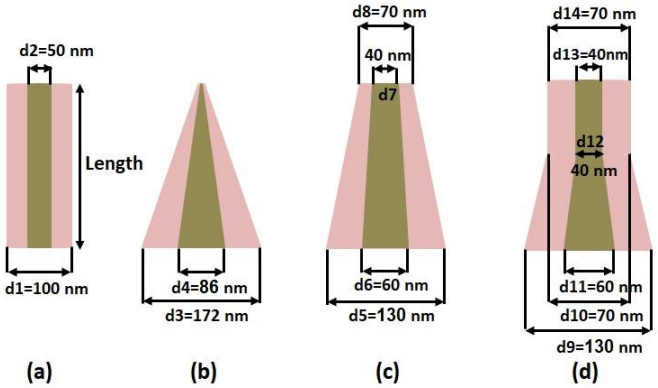

Fig. 2. 2D Schematic diagram of the proposed nanostructures.

Firstly, the SC was simulated with an optical model to obtain the absorption, photocurrent density and carriers generation rates in the active region. Then, the nanostructures (core-shell designs) were optimized using the optical model to maximize the carrier generation rate. The nanostructures suggested were added with a view to improve the hole transfer in the device, the J_{ph} and the SC efficiency - the idea of using different core-shell materials in the SC is a feature commonly associated with improved efficiency, but however, finding the appropriate materials is the problem. Here finding a new direct semiconductor material, with a suitable energy band, is the main criterion to achieve this goal and therefore, most of familiar semiconductor materials, such as Si and GaAs, are not used in this study. However, GeSe is a perfect candidate for the design proposed and it is worth noting that the light absorption through the PSC occurs at wavelengths between 300 and 800 nm – noting that half of the power of the sun lies in the wavelength band from 700 and 2500 nm. Therefore, it is highly needed to recover the wasted energy by increasing the light absorption in the PSC [53, 54].

In this study, the core-shell nanostructures have GeSe as a shell material to absorb more of the incident sunlight. This is due to the absorption spectrum of the GeSe that includes the wavelength range from 800 to 1000 nm. Moreover, the GeSe nanostructure is used to increase the light trapping through the active layer, showing improved light absorption. In order to maximize the light absorption, the photocurrent density (J_{ph}) and the generation of carriers, the different geometrical parameters were studied and performance optimized. Figure 3 shows the absorption spectra of the structures studied where it may be seen that strong absorption and high Gopt of the Perovskite are obtained over the important wavelength range from 300 nm to 800 nm. Further, there is no absorption and no carrier generation when the wavelength is larger than 800 nm. However, the proposed designs, with different NiO/GeSe core-shell nanostructures, can absorb the incident light and generate carriers in the wavelength region beyond 800 nm. This arises from the light trapping, due to the nanostructures suggested, in the active layer. Therefore, the optical path length and hence the light absorption and J_{ph} are increased. In the proposed design, the GeSe has been utilized as a complementary material to overcome the low absorption, through the wavelength range from 800 nm to 1000 nm. The absorption achieved in the 800-1000 nm range agrees well with that reported in [55].

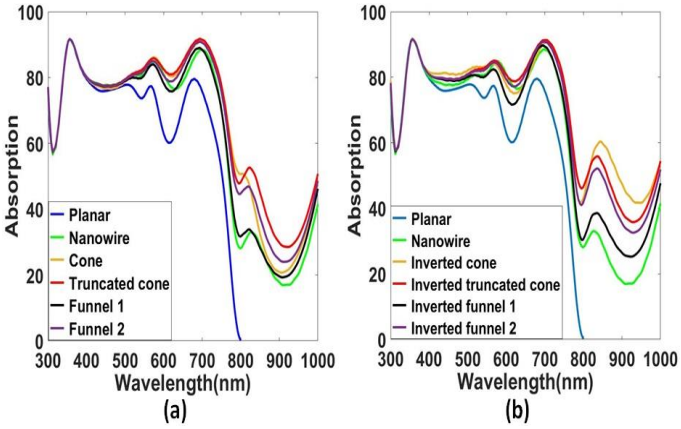

Fig.3. The light absorption of the planar PSC and PSC with (a) nanostructures and (b) inverted nanostructures proposed.

The highest absorption improvement is obtained with the use of an inverted cone core-shell, while the lowest absorption improvement is obtained for the nanowire core-shell, because the cylindrical nanowire has an essential antireflection effect that boosts the absorption in the short wavelength range, and supports only the low-order modes. The conical NW offers the multiple optical resonances which are crucial for broadband absorption. The conical nanowires (CNWs) produce a graded refractive index across the Perovskite to the core-shell interface to repress the Fresnel reflection over a wide range of wavelengths. The CNWs display a 'tradeoff' between the transmission and the reflection with a larger base diameter and smaller top diameter. It has been shown that the inverted nanocone and inverted truncated cone have superior absorption, due to transmission from the larger base and antireflection from the smaller tip. There is a strong antireflection across the wide spectral ranges from 600 nm to 1000 nm, due to the effects of diffraction and the graded index. This absorption improvement can be understood from the fact that as the top of the CNW gradually decreases, more light can be directly irradiate the side of the CNW and is fully absorbed by the active material. The CNWs have linear gradient radii that can produce multiple optical resonances, which are important to the improvement of the broadband absorption. The incident light can be efficiently coupled into the active material at cross-sectional areas of various radii in the design suggested, achieving a longer optical path length– consequently the absorption and hence the photocurrent density are improved.

Figures 4(a)–4(j) show the electric field profiles of the nanostructures proposed, at λ= 900 nm. It is obvious from these figures that the concentration of the electric field of the proposed nanostructures is stronger than for the planar PSC. Therefore, the incident light has an intense penetration and confinement through the designs proposed. There is no absorption in the Perovskite beyond a wavelength of ~800 nm and therefore no carriers are generated. In contrast, beyond a wavelength of ~800 nm, the NiO/GeSe core-shell nanostructures start to absorb the incident light, and hence generate carriers. The light is trapped and interacts with the nanostructures when the wavelength is increased to ~1000 nm. This interaction is improved and the variations in the absorption are boosted, leading to the carrier generation increasing, as shown in Fig. 4. Since the absorption is not happening in the active material over the wavelength range from 800 to 1000 nm, the GeSe is used to overcome this issue.

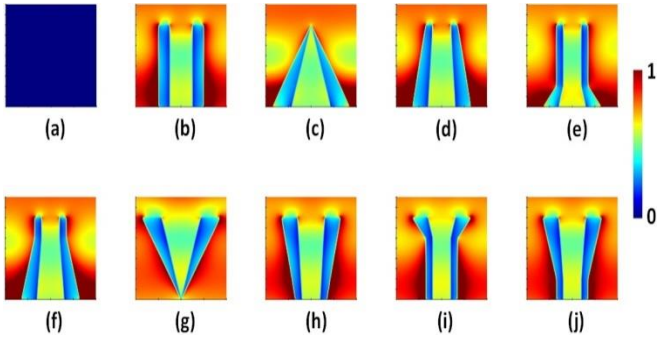

Fig.4. Absorption field profiles of (a) planar PSC, (b) nanowire core-shell, (c) cone core-shell, (d) truncated cone core-shell, (e) first funnel core-shell, (f) second funnel core-shell, (g) inverted cone core-shell, (h) inverted truncated cone, (i) inverted funnel 1, and (j) inverted funnel 2, at λ= 900 nm.

In this study, one of the aims of using the nanostructures proposed in the PSC is to improve the carrier transfer and collection. The lengths of the nanostructures studied are as shown in Fig. 5, illustrating the photocurrent density (J_{ph}) as a function of length of the core-shell nanostructures for different designs. Fig. 5(a) shows the photocurrent density enhancement over the planar PSC, using the core-shell nanostructures proposed, of different lengths in the range from 60 nm to 160 nm. By increasing the length of the core-shell of the nanostructures up to 160 nm, the optical light trapping will be increased through the active layer and hence the light absorption, J_{ph} and generation of carriers will be increased. Due to the presence of the nanostructures, the light is trapped between the two structures of the core-shell, which improves the light absorption inside the active layer and thereby the value of J_{ph} and G_{opt} will be increased. The light within the active layer is also reflected, and this reflection is referred to as the 'effective reflection'. According to this figure, it is easy to deduce that increasing the height of the core-shell can decrease the recombination rate, resulting in the increase of J_{ph}. It may be seen that photocurrent density was increased to 23.86 mA/cm^2 using a cylindrical NW design, with an enhancement of 27.59 % compared to the planar PSC. Additionally, an enhancement of 35.50 % was achieved using a conical core-shell design. Further, the photocurrent density was improved by ~40% by using the truncated cone nanostructure. Fig. 5(b) illustrates the photocurrent density achieved by using inverted nanostructures. Further, by employing the inverted conical core-shell, the J_{ph} enhancement achieved is equal to 45.61 % and the inverted truncated cone also improves the value of J_{ph} by 44.49 %. These effects of adding funnel and inverted funnel shaped core shell nanostructures are also shown in Figs. 4 and 5.

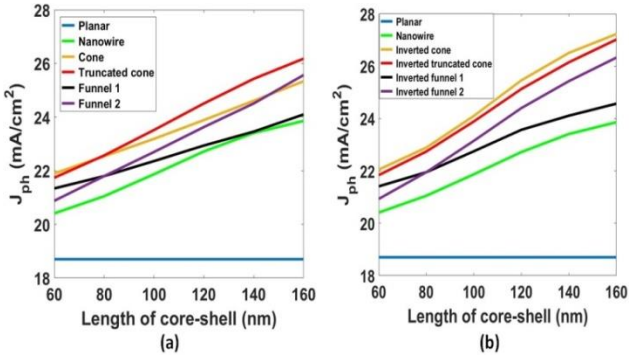

Fig.5. Variation of the photocurrent density (J_{ph}) of the proposed SCs with the length of the nanostructures.

The combination of the lower and higher order modes, from the cylinder and the tapered cone design, results in the multiple optical resonances required for broadband absorption. The geometrical parameters used are listed in Table 2. The funnel-shaped NW consists of two structures. The first is a truncated cone with length of 40 nm and a cylindrical structure, over which its length changes from 20 nm to 120 nm. The second funnel-shaped NW also has a cylindrical structure of length 40 nm, while the truncated cone length changes from 20 nm to 120 nm. As shown in Fig. 5, the photocurrent density is can be noted to be enhanced by 28.87 %, 36.73%, 31.39%, and 40.80 % by using the following: the first funnel, the second funnel, inverted funnel 1, and inverted funnel 2, respectively. The maximum photocurrent density has been attained at a length of 160 nm, and thus it will be used in the next steps in the work.

Figure 6 shows the calculated optical generation rate for the planar PSC and the proposed core-shell nanostructures. The absence of nanostructures in the active layer requires the holes to go a long way to reach the HTL, and this leads to an increase in the probability of the recombination in the SC and subsequently the transfer of the carriers does not occur properly. Also, the presence of the nanostructures inside the active layer helps the holes to travel over a shorter path than in the previous case in the conventional PSC and thus reach the HTL more rapidly. It is found that the generation rate is maximum at the interface between the nanostructures and the host material, which is due to the possible multiple light reflection that occurs with the nanostructures inside the active region. Going down inside the active region, the generation rate decreases too much because the Perovskite layer has absorbed most of the incident light, while the light is trapped between the adjacent nanostructures. Figure 7 shows the effect of varying the shell diameter of the proposed nanostructures, where in this investigation, the other parameters of the nanostructures are kept constant. It can be seen from Fig.7 that the photocurrent density behavior decreases with the shell diameter variation, by the length of the diameter decreasing. Additionally, the photocurrent densities of the structures have minimum values of 22.57 mA/cm^2, 23.20 mA/cm^2, 23.54 mA/cm^2, 23.66 mA/cm^2, 23.16 mA/cm^2, 23.24 mA/cm^2, 23.40 mA/cm^2, 23.54 mA/cm^2 for the cone, the inverted cone, the truncated cone, the inverted truncated cone, funnel 1, inverted funnel 1, funnel 2, and inverted funnel 2, respectively. As the shell diameter of the conical part decreases, the linear gradient radius decreases as well, leading to a weak generation of multiple optical resonances that is crucial for the absorption improvement. The coupling, and hence the penetration of the incident light with different wavelengths through the active material, decreases. Therefore, the longer optical path length required, such as that occurring through the cylindrical NWs, cannot be achieved. Consequently, the absorption has decreased and the reflection has increased, leading to a decreasing of the value of J_{ph}.

4. CONCLUSIONS

In this paper, a major study has been carried out into various core-shell nanostructures of NiO/GeSe, where the HTL was introduced and designed for the PSC. To address this aim, the GeSe studied was utilized in the form of a nanostructure as a complementary active material to enhance the absorption and thus the generation of carriers at wavelengths >800 nm. However, as the hole injection efficiency of this material is low, NiO was used as the core to facilitate the transfer of holes from GeSe to CuSCN, and hereby a new form of NiO/GeSe core-shell nanostructure was attained. The performance of the PSC based on these nanostructures was studied via the 3D-optical model in which the mechanisms of carrier transfer and collection, and the height of core-shell nanostructures, were taken into account. The optimum height of the core-shell was found to be 160 nm, with an identical value of J_{ph} (equal to 27.23 mA/cm^2), using the inverted cone nanostructure.

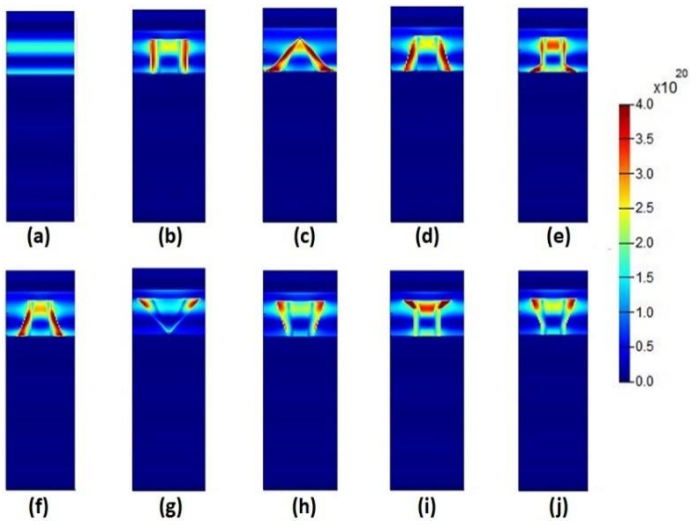

Fig.6. Profiles for the optical generation rate (G_{OPT}) at λ= 650 nm (a) planar PSC, (b) nanowire core-shell, (c) cone core-shell, (d) truncated cone core-shell, (e) first funnel core-shell, (f) second funnel core-shell, (g) inverted cone core-shell, (h) inverted truncated cone, (i) inverted funnel 1, and (j) inverted funnel 2.

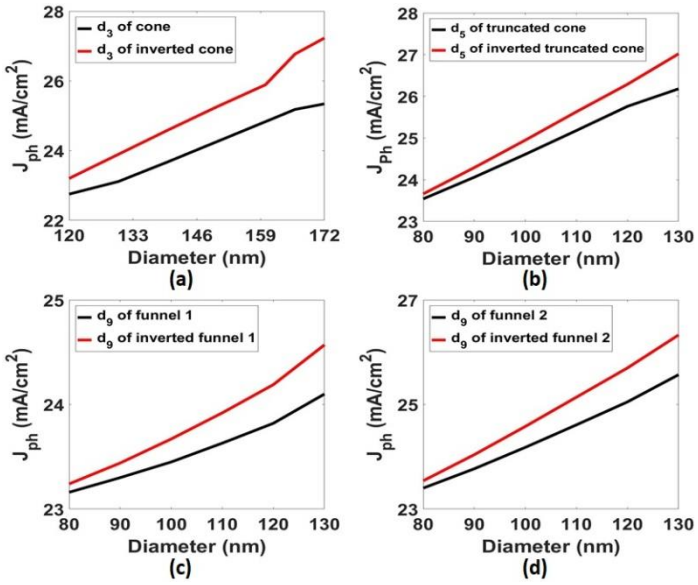

Fig.7. Photocurrent density of the nanostructures at (a) conical NWs (b) truncated cone NWs (c, d) funnel NWs.

Acknowledgments

The authors acknowledge the financial support by "Science, Technology and Innovation Funding Authority" (STIFA) at Egypt under the Institutional Links Grants. Egypt-UK Cooperation: Newton Mosharafa Program with Project ID: 30732". Grattan acknowledges support from the Royal Academy of Engineering (UK).

Disclosures

The authors declare that there are no conflicts of interest related to this article.

References

1. S. Wang, B. D. Weil, Y. Li, K. X. Wang, E. Garnett, S. Fan, and Y. Cui, “Large-area free-standing ultrathin single crystal silicon as processable materials, ”Nano Lett. 13(9), 4393– 4398(2013).
2. S.Jeong, M. D. McGehee, and Y. Cui, “All-back-contact ultra-thin silicon nano cone solar cells with 13.7% power conversion efficiency, ”Nat. Commun. 4(1), 2950(2013).
3. K. A. Catchpole and A. Polman, “Plasmonic sola rcells,”Opt. Express 16(26), 21793–21800 (2008).
4. T. G. Chen, P. Yu, S. W. Chen, F. Y. Chang, B. Y. Huang, Y. C. Cheng, J. C. Hsiao, C. K. Li, and Y. R. Wu, “Characteristics of large-scale nanohole arrays for thin-silicon photovoltaics,” Prog. Photovolt: Res. Appl.22(4), 452–461(2014).
5. J. Vukajlovic-Plestina, W. Kim, L. Ghisalberti, G. Varnavides, G. Tütüncuoglu, H. Potts, M. Friedl, L. Güniat, W. Carter, V. Dubrovskii, and A. F. I Morral, “Fundamental aspects to localize self-catalyzed III-V nanowires on silicon,” Nat. Commun. 10(1), 869(2019).
6. C. M. Hsu, S. T. Connor, M. X. Tang, and Y. Cui, “Wafer-scale silicon nanopillars and nanocones by Langmuir–Blodgett assembly and etching, ”Appl. Phys. Lett. 93(13), 133109(2008).
7. A. Khaled, M. F. O. Hameed, B. M. A. Rahman, K. T. V. Grattan, S. S. A. Obayya, and M. Hussein, “Characteristics of silicon nanowire solar cells with a crescent nanohole,” Opt. Exp., vol. 28, no. 21, p. 31020, Oct. 2020, doi: 10.1364/oe.397051.
8. A. H. K. Mahmoud, M. Hussein, M. F. O. Hameed, M. Abdel-Aziz, H. M. Hosny, and S. S. A. Obayya, “Optoelectronic performance of a modified nanopyramid solar cell, ”J. Opt. Soc. Am. B 36(2), 357–365(2019).
9. F. M. Korany, M. F. O. Hameed, M. Hussein, R. Mubarak, M .I . Eladawy, and S. S. A. Obayya, “Conical structures for highly efficient solar cell applications, ”J. Nanophotonics 12(01), 1(2018).
10. G. Y. Abdel-Latif, M. F. O. Hameed, M. Hussein, M. Abdel Razzak, andS. S. A. Obayya, “Characteristics of highly efficient star-shaped nanowires solar cell, ”J. Photonics Energy 8(04), 1(2018).
11. Raman, Aaswath, Yu, Zongfu, Fan, Shanhui, 2011. Dielectric nanostructures for broadband light trapping in organic solar cells. Opt. Exp. 19 (20), 19015–19026.
12. Yang, Z., Gao, P., Zhang, C., Li, X., Ye, J., 2016. Scattering effect of the high-index dielectric nanospheres for high performance hydrogenated amorphous silicon thin-film solar cells. Sci. Rep. 26(6), 30503.
13. M. A. Elrabiaey, M. Hussein, M. F. O. Hameed, and S. Obayya, “Light absorption enhancement in ultrathin film solar cell with embedded dielectric nanowires,” Sci. Rep. 10, 17534 (2020).
14. A.A. Mohsen, M. Zahran, S.E.D. Habib, N.K. Allam, “Refractory plasmonics enabling 20% efficient lead-free perovskite solar cells”. Sci. Rep., 10 (2020), p. 6732.
15. K. Kumar, U. K. Kumawat, R. Mital, and A. Dhawan, “Light trapping plasmonic butterfly-wing-shaped nanostructures for enhanced absorption and efficiency in organic solar cells,” J. Opt. Soc. Am. B 36(4), 978–990 (2019).
16. Sachchidanand and D. P. Samajdar, “Light-trapping strategy for PEDOT:PSS/c-Si nanopyramid based hybrid solar cells embedded with metallic nanoparticles,” Sol. Energy, vol. 190, pp. 278–285, Sep. 2019, doi: 10.1016/j.solener.2019.08.023.
17. J. He, W. Zhang, J. Ye, and P. Gao, “16% efficient silicon/organic heterojunction solar cells using narrow band-gap conjugated polyelectrolytes based low resistance electron-selective contacts,” Nano Energy, vol. 43, pp. 117–123, 2018.
18. X. Duan, X. Zhang, Y. Zhang, “High performance organic-nanostructured silicon hybrid solar cell with modified surface structure Nanoscale” Res. Lett., 13 (1) (2018), p. 283.
19. Yang, M., Zhou, Y., Zeng, Y., Jiang, C.S., Padture, N.P., Zhu, K., 2015. Square-centimeter solution-processed planar $CH_3NH_3PbI_3$ perovskite solar cells with efficiency exceeding 15%. Adv. Mater. 27 (41), 6363–6370.
20. Fei, C., Li, B., Zhang, R., Fu, H., Tian, J., Cao, G., 2017. Highly efficient and stable perovskite solar cells based on monolithically grained $CH_3NH_3PbI_3$ film. Adv. Energy Mater. 7 (9).
21. Zhong, M., Chai, L., Wang, Y., 2019. Core-shell structure of ZnO@ TiO_2 nanorod arrays as electron transport layer for perovskite solar cell with enhanced efficiency and stability. Appl. Surf. Sci. 464, 301–310.
22. Arora, N., et al., 2017. Perovskite solar cells with CuSCN hole extraction layers yield stabilized efficiencies greater than 20%. Science 358 (6364), 768–771.
23. Grätzel, M., 2014. The light and shade of perovskite solar cells. Nat. Mater. 13 (9), 838.
24. Park, N.-G., Miyasaka, T., Grätzel, M., 2016. Organic-inorganic Halide Perovskite Photovoltaics. Springer, Cham, Switzerland.
25. Bisquert, J., Juarez-Perez, E.J., 2019. The Causes of Degradation of Perovskite Solar Cells. ACS Publications.
26. National renewable energy laboratory: photovoltaic research [WWW Document], 2021. URL https://www.nrel.gov/pv/ (accessed 1.28.21).
27. M.H. Mohammadi, D. Fathi, M. Eskandari. NiO@ GeSe core-shell nano-rod array as a new hole transfer layer in perovskite solar cells: A numerical study. Sol. Energy, 204 (2020), pp. 200-207.
28. Hou, G.-J., Wang, D.-L., Ali, R., Zhou, Y.-R., Zhu, Z.-G., Su, G., 2018. $CH_3NH_3PbI_3$/GeSe bilayer heterojunction solar cell with high performance. Sol. Energy 159, 142–148.
29. Ulaganathan, R.K., et al., 2016. High photosensitivity and broad spectral response of multi-layered germanium sulfide transistors. Nanoscale 8 (4), 2284–2292.
30. Yang, X., Wang, H., Cai, B., Yu, Z., Sun, L., 2018. Progress in hole-transporting materials for perovskite solar cells. J. Energy Chem. 27 (3), 650–672.
31. Zhang, J., et al., 2018. Solution-processed Sr-doped NiOx as hole transport layer for efficient and stable perovskite solar cells. Sol. Energy 174, 1133–1141.
32. Sajid, S., et al., 2018. Breakthroughs in NiOx-HTMs towards stable, low-cost and efficient perovskite solar cells. Nano Energy 51, 408–424.
33. Chang, W., Tian, H., Fang, G., Guo, D., Wang, Z., Zhao, K., 2019. Simulation of innovative high efficiency perovskite solar cell with Bi-HTL: NiO and Si thin films. Sol. Energy 186, 323–327.
34. Grätzel, M., 2014. The light and shade of perovskite solar cells. Nat. Mater. 13 (9), 838.
35. Arora, Neha, Ibrahim Dar, M., Hinderhofer, Alexander, Pellet, Norman, Schreiber, Frank, Zakeeruddin, Shaik Mohammed, Grätzel, Michael, 2017. Perovskite solar cells with CuSCN hole extraction layers yield stabilized efficiencies greater than 20%. Science eaam5655.
36. Luo, Q., Deng, X., Zhang, C., Yu, M., Zhou, X., Wang, Z., Chen, X., Huang, S., 2018. Enhancing photovoltaic performance of perovskite solar cells with silica nanosphere antireflection coatings. Sol. Energy 15 (169), 128–135.
37. Zeng, Xiaofeng, Zhou, Tingwei, Leng, Chongqian, Zang, Zhigang, Wang, Ming, Hu, Wei, Tang, Xiaosheng, Lu, Shirong, Fang, Liang, Zhou, Miao, 2017. Performance improvement of perovskite solar cells by employing a CdSe quantum dot/PCBM composite as an electron transport layer. J. Mater. Chem. A 5 (33), 17499–17505.
38. Paetzold, U.W., Qiu, W., Finger, F., Poortmans, J., Cheyns, D., 2015. Nanophotonic front electrodes for perovskite solar cells. Appl. Phys. Lett. 106 (17), 173101.
39. Adhyaksa, G.W., Johlin, E., Garnett, E.C., 2017. Nanoscale back contact perovskite solar cell design for improved tandem efficiency. Nano Lett. 17 (9), 5206–5212.
40. Spinelli, P., Verschuuren, M.A., Polman, A., 2012. Broadband omnidirectional antireflection coating based on subwavelength surface Mie resonators. Nat. Commun. 21(3), 692.
41. Raman, Aaswath, Yu, Zongfu, Fan, Shanhui, 2011. Dielectric nanostructures for broadband light trapping in organic solar cells. Opt. Exp. 19 (20), 19015–19026.

42. Ren, Rui, Zhong, Zheng, 2018. Enhanced light absorption of silicon solar cells with dielectric nanostructured back reflector. Opt. Commun. 417, 110–114.
43. Jin, I.S., Lee, J.H., Noh, Y.W., Park, S.H., Jung, J.W., 2019. Molecular doping of CuSCN for hole transporting layers in inverted-type planar perovskite solar cells. Inorg. Chem. Front. 6 (8), 2158–2166.
44. Abdelraouf, O.A., Allam, N.K., 2016. Towards nanostructured perovskite solar cells with enhanced efficiency: Coupled optical and electrical modeling. Sol. Energy 137, 364–370.
45. He, M. et al., 2014. High efficiency perovskite solar cells: from complex nanostructure to planar heterojunction. J. Mater. Chem. A 2, 5994–6003.
46. https://www.lumerical.com/
47. Baum, M., Alexeev, I., Latzel, M., Christiansen, S.H., Schmidt, M., 2013. Determination of the effective refractive index of nanoparticulate ITO layers. Opt. Express 21 (19), 22754–22761.
48. Pattanasattayavong, P., et al., 2013a. Electric field-induced hole transport in copper (I) thiocyanate (CuSCN) thin-films processed from solution at room temperature. Chem. Commun. 49 (39), 4154–4156.
49. Ball, J.M., et al., 2015. Optical properties and limiting photocurrent of thin-film perovskite solar cells. Energy Environ. Sci. 8 (2), 602–609.
50. Wang, X., Wu, G., Zhou, B., Shen, J., 2013. Optical constants of crystallized TiO_2 coatings prepared by sol-gel process. Materials 6 (7), 2819–2830.
51. Souri, D., Salehizadeh, S.A., 2009. Effect of NiO content on the optical band gap, refractive index, and density of TeO2–V2O5–NiO glasses. J. Mater. Sci. 44 (21), 5800–5805.
52. Eymard, R., Otto, A., 1977. Optical and electron-energy-loss spectroscopy of GeS, GeSe, SnS, and SnSe single crystals. Phys. Rev. B 16 (4), 1616.
53. Green, M.A., Ho-Baillie, A., Snaith, H.J., 2014. The emergence of perovskite solar cells. Nat. Photonics 8 (7), 506.
54. Santamouris, M., 2012. Advances in Passive Cooling. Routledge.
55. M. Aliyariyan, D. Fathi, M. Eskandari, A. Tooghi. Efficiency enhancement of perovskite solar cells by designing GeSe nanowires in the structure of the adsorbent layer. Nanotechnology, 31 (46) (2020) 465405.